Available online at www.sciencedirect.com
SCIENCE DIRECT®
International Journal of Heat and Mass Transfer 47 (2004) 3507–3515
International Journal of HEAT and MASS TRANSFER
www.elsevier.com/locate/ijhmt

Inverse determination of surface temperature in thin-film/substrate systems with interface thermal resistance

Shih-Kuo Wu, Hsin-Sen Chu *

Department of Mechanical Engineering, National Chiao Tung University, Hsinchu 300, Taiwan, ROC

Received 15 November 2003; received in revised form 5 January 2004

Abstract

This work examines the effect of interface thermal resistance on the estimation of surface temperatures in thin-film/substrate systems. A radiation-boundary-condition model based on the acoustic mismatch model (AMM) is employed to consider the interface thermal resistance between thin-film and substrate. The inverse heat conduction problem is solved using the space-marching technique. The influences of interface thermal resistance, measurement locations, and measurement errors on this method are studied in detail. Numerical results show that the inverse method accurately estimates surface conditions and temperature distributions in a two-layer system even with an abrupt temperature drop at the interface. Sensor locations and interface thermal resistance only slightly affect the accuracy of the inverse estimation during the transient process when the exact input data (without measurement errors) are applied. However, the inaccuracy might be amplified by the interface thermal resistance and sensor locations if measurement errors exist.

1. Introduction

Thin-film/substrate systems are widely used in superconducting bolometers, microelectronics systems, and electro-optic devices. In such systems it is often necessary to know surface temperatures and temperature distributions within the media. These temperature profiles can be calculated if material thermal properties, initial and boundary conditions are given. However, in some circumstances, boundary conditions are difficult to determine. For example, if the surface of the thin-film is suffering laser heating, it is unsuitable for attaching a sensor on the surface. Hence, temperature detectors are placed inside the substrate. Use of the inverse methods allows determination of thermal properties and estimation of temperature distributions and unknown boundary conditions by means of internal or external measurements [1].

Over the past three decades, a considerable amount of work has been done on the study of inverse heat transfer problems by either analytical methods or numerical methods. The analytical methods include exact methods, polynomial methods, and integral methods [2]. These methods are only useful for solving linear one-dimensional problems with particular initial and boundary conditions. Numerical methods, on the other hand, have the advantage of being applicable to any problem type.

The intrinsic characteristic of inverse problems is that they are ill-posed [2]. By contrast, a well-posed problem meets the following three requirements: existence, uniqueness and stability. It has been proved that solutions to inverse heat conduction problems usually exist and are unique. However, the obtained estimates are not always numerically stable. In other words, small inaccuracies in the measured interior temperatures may cause large oscillations in the calculated surface conditions. Thus, many special methods have been proposed to solve inverse heat conduction problems (IHCPs). The main purpose of these inverse methods is to improve the stability of numerical calculation results.

Interface thermal resistance plays an important role in determining heat flow in thin-film/substrate systems. For example, a restriction in heat flow from the superconducting film can cause a transition from the

* Corresponding author. Tel.: +886-3-5712121x55115; fax: +886-3-5727930.
E-mail address: hschu@cc.nctu.edu.tw (H.-S. Chu).

0017-9310/$ - see front matter © 2004 Elsevier Ltd. All rights reserved.
doi:10.1016/j.ijheatmasstransfer.2004.01.022

Nomenclature

C_p	specific heat [kJ/kg K]
E_{int}	estimation error at the interface, $\lvert T_{\text{est}} - T_{\text{exa}}\rvert / T_{\text{exa}}$
k	thermal conductivity [W/mK]
L	system thickness [m]
L_1	interface location [m]
L_r	first sensor location [m]
q	heat flux [W/m^2]
Q	dimensionless heat flux, Lq/kT_L
t	time [s]
T	temperature [K]
T_0	initial temperature [K]
T_L	temperature of the left surface [K]
x	spatial coordinate [m]
Y_1, Y_2	temperature histories at the first and second sensor locations

Greek symbols

α	thermal diffusivity [m^2/s]
$\Delta\theta$	dimensionless temperature difference in the interface
θ	dimensionless temperature, T/T_L
κ	constant; see Eq. (5)
ξ	dimensionless space coordinate, x/L
ξ_1	dimensionless interface location, L_1/L
ξ_r	dimensionless first sensor location, L_r/L
ρ	density [kg/m^3]
σ	bound of random error
τ	dimensionless time, $\alpha_1 t/L^2$
ϖ	random error

Subscripts

0	initial condition
est	estimated
exa	exact
i	grid space index
j	layer index; 1 represents layer 1, 2 represents layer 2

Superscripts

m	final time
n	time index

superconducting state to the normal state during operation of the device, resulting in device failure. Recently, interface thermal resistance has received special interest and attention in many fields such as microelectronics systems [3], superlattices [4,5], and superconductor film/substrate composites [6–9]. Many experiments have been conducted to determine the interface thermal resistance between thin films and substrates. Nahum et al. [10] directly measured the interface thermal resistance over the temperature range 97 K $\leqslant T \leqslant$ 177 K for Y–Ba–Cu–O films deposited on sapphire with and without various intervening buffer layers. The thermal contact resistance can also be indirectly estimated from the measured time constant of the transient voltage response to a heat or optical input [11,12]. Leung et al. [13] predicted the thermal contact conductance in vacuum using statistical mechanics. Kelkar et al. [14] discussed the effect of heat flux on the interface thermal resistance.

In addition to experimental quantification of interface thermal resistance, theoretical analysis also has been done by many researchers. The interfacial layer model assumes an ultra-thin layer with very low conductance exists between two dissimilar materials. Two important parameters directly and significantly affecting the magnitude of the resistance are the conductivity and thickness ratios of interfacial layer to film, respectively. Little [15] predicted interface thermal resistance by treating phonons as plane waves and proposed the acoustic mismatch model (AMM). An essential assumption of the AMM is that no scattering occurs at the interface. Swartz and Pohl [16] considered the diffuse scattering occurring at the interface and proposed the diffuse mismatch model (DMM). The AMM and DMM are both in the same form as the radiation boundary condition, in which the heat flow across the interface is proportional to the fourth power of the temperature on each side of the interface. The applicability of AMM or DMM has been discussed in detail by Phelan [17]. In this work, the results showed that the applicability of AMM and DMM is determined by the ratio λ_d/δ, where λ_d is the dominant phonon wavelength, and δ is the mean interfacial roughness. When $\lambda_d/\delta \gg 1$, the AMM is applicable, otherwise, the DMM applies. Recently, Zeng and Chen [18] examined the applicability of the thermal boundary resistance to the case with internal heat generation. Prasher and Phelan [19] developed a model, called the scattering-mediated acoustic mismatch model (SMAMM), to exploit the analogy between phonon and radiative transport by developing a damped wave equation to describe the phonon transport. More recently, Chantrenne and Raynaud [20] developed the simulations of heat transfer through an interface by molecular dynamics.

Thus, determining surface temperatures in thin-film/substrate systems with interface thermal resistance has become a very important issue. To the best of the authors' knowledge, no work has thoroughly investigated the inverse estimation of surface temperatures in thin-film/substrate systems with interface thermal resistance. In this study, a space-marching technique [21] is adopted to

estimate the temperature distributions and unknown boundary conditions from internal measurements. A radiation-boundary-condition model based on the AMM is employed to consider the interface thermal resistance between the thin-film and substrate. The influences of interface thermal resistance, measurement errors, and measurement locations are studied. Furthermore, the results of the estimation for the cases with or without interface thermal resistance are also compared.

2. Analysis

2.1. Direct problem formulation

Consider one-dimensional conductive heat transfer in a two-layer medium as illustrated in Fig. 1. The temperature of the medium is initially T_0. At time $t = 0$, the temperature at $x = 0$ has risen to T_L while the temperature at $x = L$ is still T_0. All thermal properties in this study are assumed to be temperature-independent. For convenience in the subsequent analysis, nondimensional variables are defined as follows:

$$\theta_j = \frac{T_j}{T_L}, \quad \tau = \frac{\alpha_1 t}{L^2}, \quad \xi = \frac{x}{L}, \quad \xi_1 = \frac{L_1}{L}, \quad \xi_r = \frac{L_r}{L}, \quad Q_j = \frac{Lq_j}{k_j T_L}, \tag{1}$$

where α is the thermal diffusivity and k is the thermal conductivity. The subscript j represents Layer j, where $j = 1$ or 2. The governing equations for this problem are

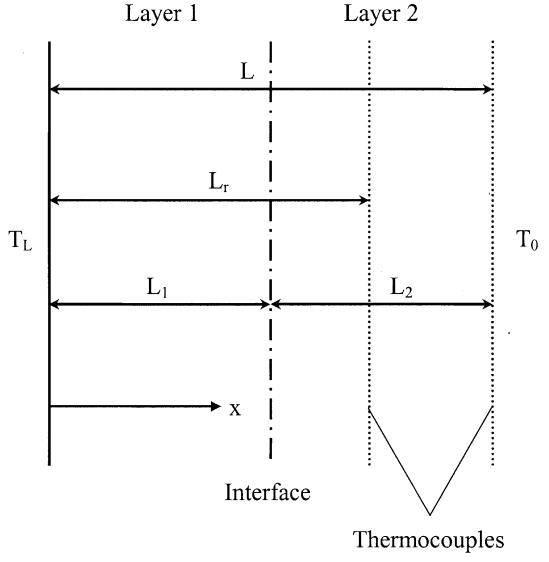

Fig. 1. Schematic diagram of the physical system.

$$\frac{\partial \theta_j}{\partial \tau} = \frac{\alpha_j}{\alpha_1} \frac{\partial^2 \theta_j}{\partial \xi^2}. \tag{2}$$

The initial conditions are

$$\theta_j(0, \xi) = \theta_0. \tag{3}$$

The boundary conditions are

$$\theta_1(\tau, 0) = 1, \tag{4a}$$

$$\theta_2(\tau, 1) = \theta_0. \tag{4b}$$

At the interface, the radiation-boundary-condition model is employed, thus the heat flux continuity is

$$\frac{\partial}{\partial \xi} \theta_1(\tau, \xi_1) = \frac{k_2}{k_1} \frac{\partial}{\partial \xi} \theta_2(\tau, \xi_1) = -\frac{LT_L^3}{k_1} \kappa [\theta_1^4(\tau, \xi_1) - \theta_2^4(\tau, \xi_1)], \tag{5}$$

where κ is a function of the material properties of the two media in contact. Higher κ represents less interface thermal resistance.

2.2. Inverse problem formulation

The inverse heat conduction problem is to estimate the temperature histories over the whole domain from internal temperature measurements. In this study, instead of using measured temperatures, the input data for the inverse heat conduction problem are predicted from the solution of a direct problem for a given set of boundary conditions.

The set of equations for the IHCP are Eqs. (2) and (5) along with

$$\theta_1(\tau, 0) = ? \tag{6}$$

$$\theta_2(\tau, \xi_r) = Y_1(\tau) \tag{7a}$$

$$\theta_2(\tau, 1) = Y_2(\tau) \tag{7b}$$

The medium is divided into a direct and an inverse region. The problem in the direct region, $\xi_r < \xi < 1$, is a boundary-value problem with boundary conditions given by the temperature measurements Y_1 and Y_2. Y_1 and Y_2 representing the temperature history of the first sensor located at $\xi = \xi_r$ and the second sensor located at $\xi = 1$, respectively. In this study, Y_1, and Y_2 were simulated by the solution of the direct heat-transfer problem. After the temperature distributions in the direct region were obtained, the temperature distributions in the inverse region were determined by the space-marching method.

3. Numerical method

The inverse estimation is not always numerically stable, which means small inaccuracies in the measured

interior temperatures may cause large oscillations in the calculated surface conditions. Thus, many special methods have been proposed to improve the stability of numerical calculation results. The space-marching method is easy to use, accurate and stable [2]. Therefore, it was adopted to deal with the engineering problem in this manuscript. The calculations start on the boundary between direct and inverse regions and then are continued for the subsequent grids within the inverse region. The space-marching technique proposed by Raynaud and Bransier [21] uses the finite-difference method to approximate the governing equations. Central-difference approximations in space and time lead to

$$\frac{\theta_{i,j}^{n+1}-\theta_{i,j}^{n-1}}{2\Delta\tau}=\frac{\alpha_j}{\alpha_1}\frac{Q_{i-1/2,j}^{n}-Q_{i+1/2,j}^{n}}{\Delta\xi}, \tag{8}$$

where the subscripts $j=1$ or 2 represent Layer 1 or Layer 2, respectively. In addition, the dimensionless heat flux values $Q_{i-1/2,j}^{n}$ and $Q_{i+1/2,j}^{n}$ are approximated as follows:

$$Q_{i-1/2,j}^{n}=-\frac{\theta_{i,j}^{n}-\theta_{i-1,j}^{n}}{\Delta\xi}, \tag{9a}$$

$$\begin{aligned}Q_{i+1/2,j}^{n}&=\frac{1}{2}\left(Q_{i+1/2,j}^{n+1}+Q_{i+1/2,j}^{n-1}\right)\\&=-\frac{1}{2}\left[\frac{\theta_{i+1,j}^{n+1}-\theta_{i,j}^{n+1}}{\Delta\xi}+\frac{\theta_{i+1,j}^{n-1}-\theta_{i,j}^{n-1}}{\Delta\xi}\right].\end{aligned} \tag{9b}$$

It can be seen that the dimensionless heat flux $Q_{i+1/2,j}^{n}$ is the average of central-difference at times $n+1$ and $n-1$. This will decrease the sensitivity to measurement errors and stabilize the inverse method. Substituting Eqs. (9a) and (9b) into Eq. (8) results in

$$\begin{aligned}\theta_{i-1,j}^{n}=\theta_{i,j}^{n}&+\frac{\alpha_1}{\alpha_j}\frac{(\Delta\xi)^2}{2\Delta\tau}\left(\theta_{i,j}^{n+1}-\theta_{i,j}^{n-1}\right)\\&-\frac{1}{2}\left(\theta_{i+1,j}^{n+1}-\theta_{i,j}^{n+1}+\theta_{i+1,j}^{n-1}-\theta_{i,j}^{n-1}\right).\end{aligned} \tag{10}$$

The temperatures at times $n+1$ and $n-1$ are called future and past temperatures. If the temperature at time $n=N$ is desired to be calculated, the measurements should be known up to $I+N$ time steps. Here I is the number of the space grids in the inverse region. Eq. (10) cannot be used to calculate the temperature field at the final time step since it includes future temperatures. Thus, an explicit scheme that does not include future temperatures, proposed by D'Souza [22], is used to calculate the temperature distribution at the final time step. Backward-difference in time and central-difference in space lead to

$$\frac{\theta_{i,j}^{m}-\theta_{i,j}^{m-1}}{\Delta\tau}=\frac{\alpha_j}{\alpha_1}\frac{\theta_{i+1,j}^{m}-2\theta_{i,j}^{m}+\theta_{i-1,j}^{m}}{(\Delta\xi)^2}. \tag{11}$$

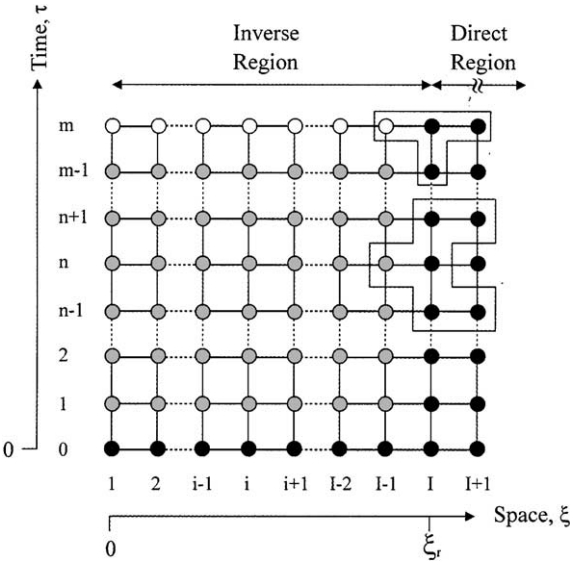

Fig. 2. Space–time grid for numerical calculations [23]: (●) temperatures estimated by Raynaud and Bransier method [21], (○) temperatures estimated by D'Souza method [22], (●) known temperatures.

Rearranging the above equation yields

$$\theta_{i-1,j}^{m}=2\theta_{i,j}^{m}-\theta_{i+1,j}^{m}+\frac{\alpha_1}{\alpha_j}\frac{(\Delta\xi)^2}{\Delta\tau}(\theta_{i,j}^{m}-\theta_{i,j}^{m-1}). \tag{12}$$

Thus, at each time step toward the unknown boundary, Eq. (10) is used for times $n=1$ to $m-1$, while Eq. (12) is used for $n=m$. The space–time grid for numerical calculations is shown in Fig. 2.

4. Results and discussion

Grid-refinement and time-step-sensitivity studies have been done to ensure the accuracy of the numerical method. In general, the accuracy of a numerical method increases as the time step decreases. However, in the inverse method sensitivity to measurement errors increases due to the smallness of the time steps. Thus, a trade-off between accuracy and stability exists. In the following cases, the time step $\Delta\tau=0.01$, the grid size $\Delta\xi=0.01$, the thermal diffusivity ratio $\alpha_2/\alpha_1=0.1$, and the thermal conductivity ratio $k_2/k_1=0.1$ are employed.

Fig. 3 shows the exact and estimated temperature profiles for $\kappa=5\times10^{-4}$ over the time sequence. It can be seen that the absolute value of the slope in Layer 2 is greater than that in Layer 1 near the interface. Because k_2 is smaller than k_1 and $\frac{\partial}{\partial\xi}\theta_1(\tau,\xi_1)=\frac{k_2}{k_1}\frac{\partial}{\partial\xi}\theta_2(\tau,\xi_1)$, it is easy to determine that $\frac{\partial}{\partial\xi}\theta_2(\tau,\xi_1)$ is greater than $\frac{\partial}{\partial\xi}\theta_1(\tau,\xi_1)$. Moreover, owing to the existence of interface thermal resistance there is an abrupt temperature jump at the interface ($\xi=0.5$). In this case, the first sensor is

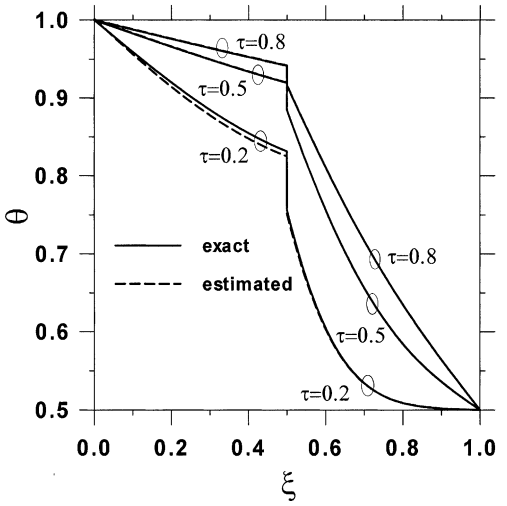

Fig. 3. Exact and estimated temperature distributions with $\kappa = 5 \times 10^{-4}$ over the time sequence.

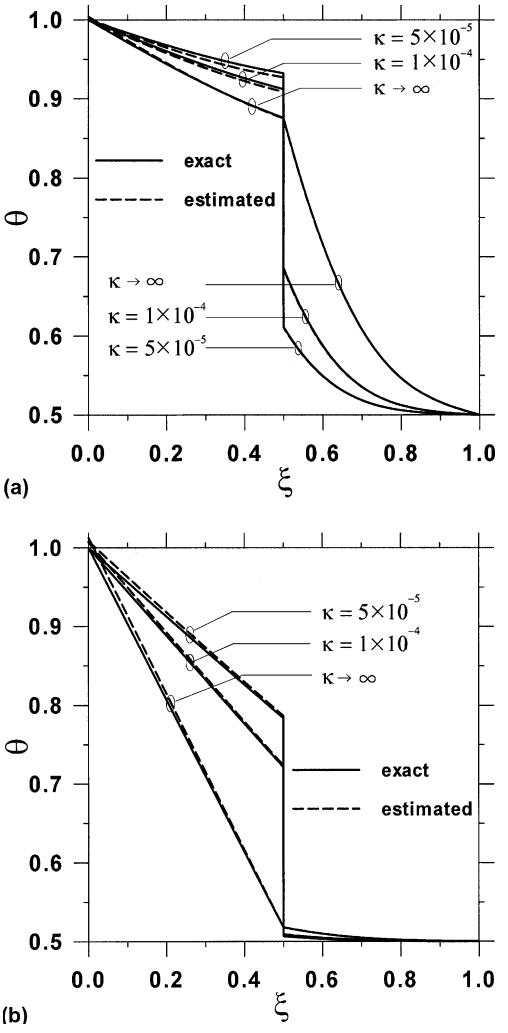

Fig. 4. Exact and estimated temperature distributions at $\tau = 0.3$ for various interface conditions with (a) $k_2/k_1 = 0.1$ and (b) $k_2/k_1 = 10$.

located at $\xi_r = 0.75$ and the second sensor is located at $\xi = 1$. Thus, $0.75 < \xi < 1$ is the direct region and $0 < \xi < 0.75$ is the inverse region. It can be seen that inverse estimation predicts well in the region $0.5 < \xi < 0.75$. The maximum relative error is about 0.7%. However, a difference between exact and estimated values appears as the calculation marches through the interface. This phenomenon is obvious for the first few time steps. For example, the estimated values did not match the exact values very well at $\tau = 0.2$ (the relative error is about 1%), but they did at $\tau = 0.5$ and $\tau = 0.8$ (the relative errors are less than 0.1%). The temperature of the left surface (unknown in the inverse problem) suddenly rose from T_0 to T_L in the direct problem. Such an abrupt temperature jump could not be predicted accurately using a numerical method. Thus, estimation accuracy is not good for the first few time steps.

Three values of κ were chosen to illustrate the effect of interface thermal resistance on the inverse solution: $\kappa = 5 \times 10^{-5}$, $\kappa = 1 \times 10^{-4}$, and $\kappa \to \infty$ (without interface thermal resistance). Fig. 4(a) depicts the exact and estimated temperature distributions within the medium at $\tau = 0.3$, with the first sensor located at $\xi_r = 0.75$. It can be seen that the differences between exact and estimated values decrease as κ increases. In other words, the accuracy of the inverse estimation increases as the interface thermal resistance decreases. Furthermore, it is interesting to note that the differences between the exact and estimated values trend toward diminution as the calculation marches through the interface to the left surface ($\xi = 0$). For example, the difference between the exact and estimated temperatures at $\xi = 0.4$, 0.3, and 0.2 are 0.005216, 0.004617, and 0.003221, respectively, for $\kappa = 5 \times 10^{-5}$. The discrepancy between the estimated and exact temperatures seems to recover as the estimated solution moves to the surface. In order to investigate this phenomenon, another case was selected to be tested. The results of the case with $k_2/k_1 = 10$ were plotted in Fig. 4(b). From Fig. 4(b), the results show that the discrepancy between the estimated and exact temperatures was slightly diverged as the estimated solution moves to the surface. However, all of these cases show that the error of inverse estimation of surface temperature is less than 1.3%.

Fig. 5 presents the exact and estimated surface temperature histories for $\kappa = 5 \times 10^{-5}$, $\kappa = 1 \times 10^{-3}$, and $\kappa \to \infty$, with $\xi_r = 0.75$. The inverse estimation solution is not good for the first few time steps, as mentioned above, however, after about 10 time steps ($\tau = 0.1$), the estimated values approach to the exact values as time elapses. In other words, the relative error decreases when

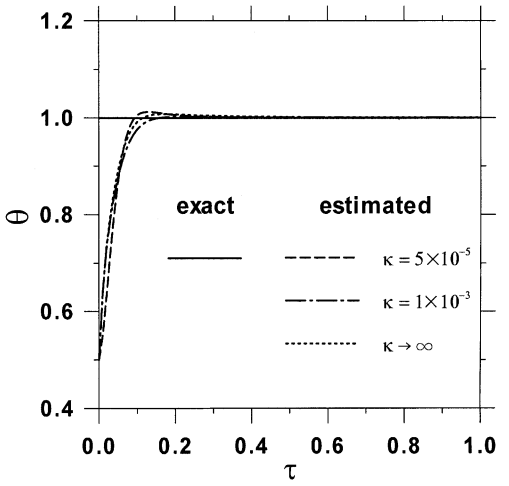

Fig. 5. Exact and estimated surface temperature histories for various interface conditions.

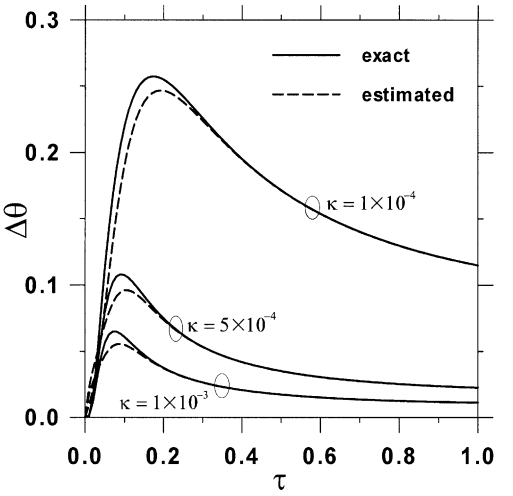

Fig. 6. Exact and estimated temperature-difference ($\Delta\theta$) histories at the interface for $\kappa = 1 \times 10^{-4}$, $\kappa = 5 \times 10^{-4}$ and $\kappa = 1 \times 10^{-3}$ with $\xi_r = 0.75$.

the time increases. The maximum relative error is about 1% at $\tau = 0.1$. Furthermore, the accuracy of the inverse method slightly increases as the interface thermal resistance decreases. However, in this case, the error is so small that it is generally not significant.

Fig. 6 shows the exact and estimated histories of the temperature difference ($\Delta\theta$) at the interface for $\kappa = 1 \times 10^{-4}$, $\kappa = 5 \times 10^{-4}$, and $\kappa = 1 \times 10^{-3}$, with $\xi_r = 0.75$. As time elapses, the temperature difference at the interface initially increases until reaching maximum then decreases to a fixed value. Thus, the steady state is reached. The small value of κ represents high interface thermal resistance that prevents heat from propagating from one material to the other, so the temperature difference at the interface decreases as κ increases. Furthermore, the moment that the maximum temperature difference appears tends to shift toward short time as κ decreases. Inverse estimation predicts this phenomenon accurately after a few time steps.

Fig. 7 illustrates the exact and estimated temperature distributions for various sensor locations, with $\kappa = 1 \times 10^{-4}$. At $\tau = 0.2$, the accuracy of the inverse estimation with $\xi_r = 0.60$ is better than that of the other two cases. The small value of ξ_r means that the sensor was located near the unknown boundary. Thus, the best inverse solution is obtained with the sensor closest to the unknown boundary. However, this phenomenon is not significant as time elapses. At $\tau = 0.6$, $\xi_r = 0.60$, $\xi_r = 0.75$, and $\xi_r = 0.90$ predict almost the same temperature distribution and they match the exact value reasonably well. The relative errors are less than 0.1% for these three cases at $\tau = 0.6$.

The maximum inverse estimation error occurs at the interface for our demonstrated case. Thus, the inverse estimation error at the interface must be thoroughly

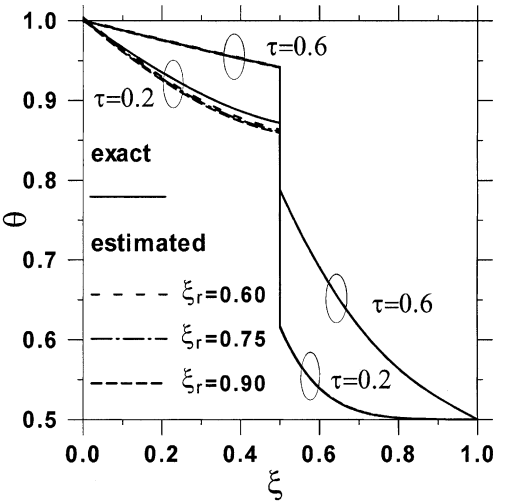

Fig. 7. Exact and estimated temperature distributions for various sensor locations with $\kappa = 1 \times 10^{-4}$.

examined. E_{int} is the absolute value of the relative error at the interface. It is chosen as an index of the inverse estimation error. Fig. 8 shows the inverse estimation error at the interface for $\kappa = 5 \times 10^{-5}$, $\kappa = 1 \times 10^{-4}$, $\kappa = 5 \times 10^{-4}$, and $\kappa \to \infty$ with $\xi_r = 0.75$. For the first few time steps such as $\tau < 0.1$, E_{int} varies sharply with time. As mentioned before, an abrupt temperature jump could not be predicted accurately using a numerical method so that the estimation accuracy is not good for the first few time steps. Furthermore, the existence of interface thermal resistance will make the estimation less accurate. Therefore, E_{int} is affected by both κ and τ. There is no general trend for E_{int} when τ is less than 0.1.

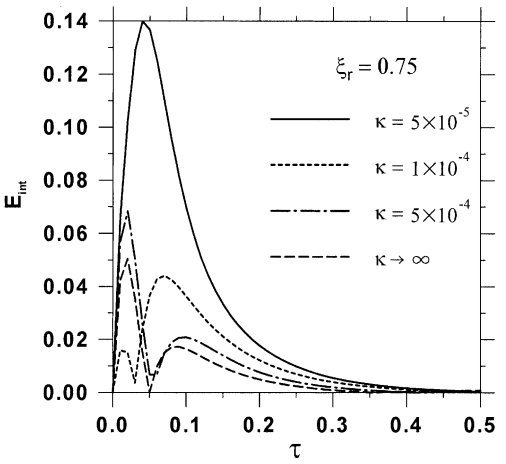

Fig. 8. Inverse estimation error at the interface for $\kappa = 5 \times 10^{-5}$, $\kappa = 1 \times 10^{-4}$, $\kappa = 5 \times 10^{-4}$ and $\kappa \to \infty$ with $\xi_r = 0.75$.

However, the results show that E_{int} decreases as κ increases after $\tau = 0.1$, i.e. less interface thermal resistance results in more accurate prediction. Besides, the figure demonstrates again that the inverse estimation error decreases as time elapses.

In order to examine the influence of sensor locations on the inverse estimation error at the interface, three different sensor location, $\xi_r = 0.60$, $\xi_r = 0.75$, and $\xi_r = 0.90$ were designated as sample cases. Fig. 9 depicts inverse estimation error at the interface for various sensor locations with $\kappa \to \infty$. It is obvious that E_{int} decreases as ξ_r increases. Thus, the inverse estimation predicts more accurately while the sensor is close to the unknown boundary.

The discussion above shows that the inverse method provides a good estimation with exact input data.

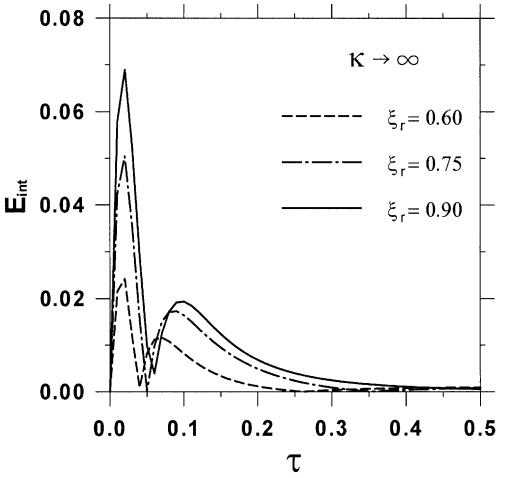

Fig. 9. Inverse estimation error at the interface for various sensor locations with $\kappa \to \infty$.

However, in practical engineering applications, measurement errors are unavoidable. Thus, the effect of measurement errors on the inverse method must be taken into account. The temperature data for the measurement locations were calculated from direct problems to simulate measurements. The simulated temperature measurements used in the inverse problems are considered to include measurement errors. In this study, random errors were added to the exact temperatures. The measured temperature T_{measured} can be expressed as

$$T_{\text{measured}} = T_{\text{exact}} + \varpi T_{\text{exact}}, \quad \varpi < |\sigma|, \tag{13}$$

where T_{exact} is the exact temperature, ϖ is the random error, and σ is the bound of ϖ.

Fig. 10 depicts the exact and estimated surface temperature histories for various sensor locations, with $\kappa = 1 \times 10^{-3}$, when measurement errors are taken into account. It can be seen that large measurement errors make the estimation less accurate. Furthermore, the inaccuracy is amplified by large ξ_r values. For the cases with exact input data (without measurement errors),

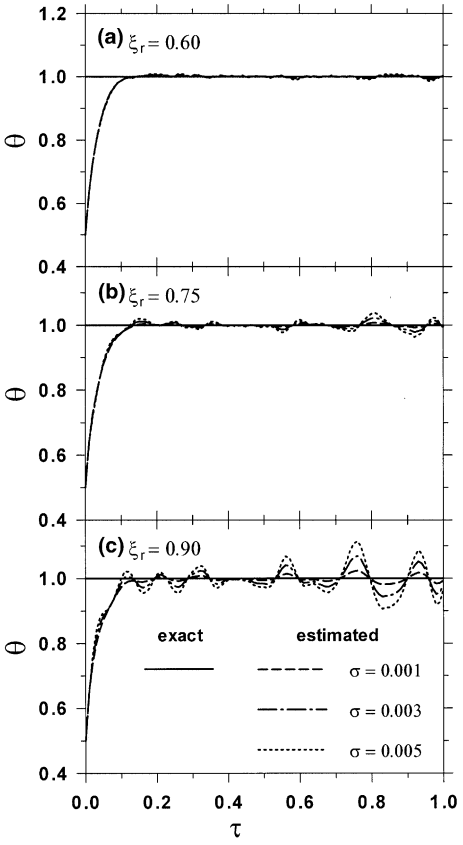

Fig. 10. Exact and estimated surface temperature histories for measurement errors 0.1%, 0.3%, and 0.5%, with $\kappa = 1 \times 10^{-3}$ with the first sensor located at (a) $\xi_r = 0.60$, (b) $\xi_r = 0.75$ and (c) $\xi_r = 0.90$.

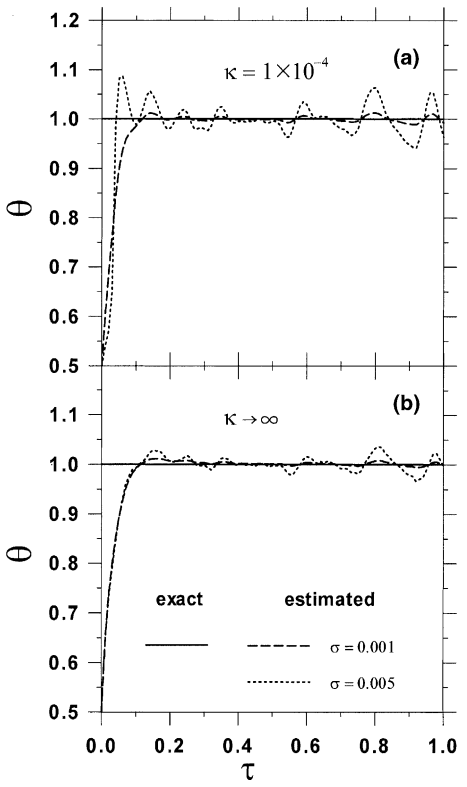

Fig. 11. Exact and estimated surface temperature histories for measurement errors 0.1% and 0.5% with interface thermal resistance: (a) $\kappa = 1 \times 10^{-4}$ and (b) $\kappa \to \infty$.

sensor locations merely slightly affect the accuracy of the inverse estimation. However, the effect will be amplified if measurement errors are taken into account. Thus, for practical engineering problems in which measurement errors are unavoidable, sensors must be located as close to unknown boundaries as possible. Fig. 11 shows an estimated surface temperature history with (a) $\kappa = 1 \times 10^{-4}$ and (b) $\kappa \to \infty$. Comparing Fig. 11(a) and (b), it is clear that the differences between exact and estimated values are amplified if when thermal resistance exists at the interface.

5. Conclusions

This paper presents a numerical analysis of estimating transient behavior of surface temperatures for thin-film/substrate systems using an inverse method. The acoustic mismatch model was employed to model the interface thermal resistance between thin-film and substrate. The space-marching technique is adopted for the analysis of the inverse heat conduction problem. Numerical results show that the inverse method accurately estimated the surface conditions and temperature distributions in a two-layer system even with an abrupt temperature drop in the interface. Sensor locations and interface thermal resistance just slightly affected the accuracy of the inverse estimation during the transient process when exact input data (without measurement errors) were applied. However, inaccuracy might be amplified by interface thermal resistance and sensor locations if measurement errors exist.

Acknowledgements

The authors would like to thank the National Science Council of Taiwan, ROC for financially supporting this research under Contract no. NSC 90-2212-E-009-073.

References

[1] J.H. Lin, C.K. Chen, Y.T. Yang, The inverse estimation of the thermal boundary behavior of a heated cylinder normal to a laminar air stream, Int. J. Heat Mass Transfer 43 (2000) 3991–4001.
[2] K. Kurpisz, A.J. Nowak, Inverse Thermal Problem, CMP, Southampton, 1996.
[3] N.J. Fisher, M.M. Yovanovich, Thermal constriction resistance of sphere/layered flat contacts: theory and experiment, ASME J. Heat Transfer 111 (1989) 249–256.
[4] G. Chen, Size and interface effects on thermal conductivity of superlattices and periodic thin-film structures, ASME J. Heat Transfer 119 (1997) 220–229.
[5] G. Chen, Thermal conductivity and ballistic-phonon transport in the cross-plane direction of superlattices, Phys. Rev. B 57 (1998) 14958–14973.
[6] P.E. Phelan, Y. Song, O. Nakabeppu, K. Ito, K. Hijikata, T. Ohmori, K. Torikoshi, Film/substrate thermal boundary resistance for an Er–Ba–Cu–O high-T_c thin film, ASME J. Heat Transfer 116 (1994) 1038–1041.
[7] R.C. Chen, J.P. Wu, H.S. Chu, Bolometric response of high-T_c superconducting detectors to optical pulses and continuous waves, ASME J. Heat Transfer 117 (1995) 366–372.
[8] P.E. Phelan, Thermal response of thin-film high-T_c superconductors to modulated irradiation, J. Thermophys. Heat Transfer 9 (1995) 397–402.
[9] R.S. Prasher, P.E. Phelan, Review of thermal boundary resistance of high-temperature superconductors, J. Supercond. 10 (1997) 473–484.
[10] M. Nahum, S. Verghese, P.L. Richards, K. Char, Thermal boundary resistance for $YBa_2Cu_3O_{7-\delta}$ films, Appl. Phys. Lett. 59 (1991) 2034–2036.
[11] C.G. Levey, S. Etemad, A. Inam, Optically detected transient thermal response of high T_c epitaxial films, Appl. Phys. Lett. 60 (1992) 126–128.
[12] C.D. Marshall, I.M. Fishman, M.D. Payer, Ultrasonic wave propagation and barrier-limited heat flow in thin films of $YBa_2Cu_3O_{7-x}$, Phys. Rev. B 43 (1991) 2696–2699.

[13] M. Leung, C.K. Hsieh, D.Y. Goswami, Prediction of thermal contact conductance in vacuum by statistical mechanics, ASME J. Heat Transfer 120 (1998) 51–57.
[14] M. Kelkar, P.E. Phelan, B. Gu, Thermal boundary resistance for thin-film high-T_c superconductors at varying interfacial temperature drops, Int. J. Heat Mass Transfer 40 (1997) 2637–2645.
[15] W.A. Little, The transport of heat between dissimilar solid at low temperature, Can. J. Phys. 37 (1959) 334–349.
[16] E.T. Swartz, R.O. Pohl, Thermal boundary resistance, Rev. Mod. Phys. 61 (1989) 605–668.
[17] P.E. Phelan, Application of diffuse mismatch theory to the prediction of thermal boundary resistance in thin-film high-T_c superconductors, ASME J. Heat Transfer 120 (1998) 37–43.
[18] T. Zeng, G. Chen, Phonon heat conduction in thin films: impacts of thermal boundary resistance and internal heat generation, ASME J. Heat Transfer 123 (2001) 340–347.
[19] R.S. Prasher, P.E. Phelan, A scattering-mediated acoustic mismatch model for the prediction of thermal boundary resistance, ASME J. Heat Transfer 123 (2001) 105–112.
[20] P. Chantrenne, M. Raynaud, Study of phonon heat conduction of metallic solids at the atomic scale, in: 12th International Heat Transfer Conference, Grenoble, France, August 2002.
[21] M. Raynaud, J. Bransier, A new finite-difference method for the nonlinear inverse heat conduction problem, Numer. Heat Transfer 9 (1986) 27–42.
[22] N. D'Souza, Numerical solution of one-dimensional inverse transient heat conduction by finite difference method, ASME Paper No. 75-WA/HT-81, 1975.
[23] N.J. Ruperti, M. Raynaud, J.F. Sacadura, A method for the solution of the coupled inverse heat conduction-radiation problem, ASME J. Heat Transfer 118 (1996) 10–17.